

**JET PHYSICS AT 2 TEV**

Mario Martínez

*Instituto de Física de Altas Energías  
Universidad Autónoma de Barcelona  
E-08193 Bellaterra (Barcelona), Spain  
CDF/PUB/JET/PUBLIC/7223*

ABSTRACT

In this contribution, a review of some of the most important QCD jet preliminary results from both CDF and D0 experiments in Run II is presented, together with future prospects as the integrated luminosity increases.

# 1 Introduction

The Run II at Tevatron will define a new level of precision for QCD studies in hadron collisions. Both collider experiments, CDF and D0, expect to collect up to  $8 \text{ fb}^{-1}$  of data in this new run period. The increase in instantaneous luminosity, center-of-mass energy (from 1.8 TeV to 1.96 TeV) and the improved acceptance of the detectors will allow stringent tests of the Standard Model (SM) predictions in extended regions of jet transverse momentum,  $P_T^{\text{jet}}$ , and jet rapidity,  $Y^{\text{jet}}$ . In this contribution, a review of some of the most important QCD results from Run II is presented, together with future prospects as the integrated luminosity increases.

## 2 Inclusive Jet Production at the Tevatron

The measurement of the inclusive jet production cross section for central jets constitutes one of the pillars of the jet physics program at the Tevatron. It provides a stringent test of perturbative QCD predictions over almost nine orders of magnitude and probes distances up to  $\sim 10^{-19}\text{m}$ . Thanks to the increase in the center-of-mass energy in Run II the jet production rate has been multiplied (by a factor of five for jets with  $P_T^{\text{jet}} > 600 \text{ GeV}$ ) and the first measurements have already extended the  $P_T^{\text{jet}}$  coverage by 150 GeV compared to Run I. In addition, both CDF and D0 experiments explore new jet algorithms, following the theoretical work that indicates that the cone-based jet algorithm employed in Run I is not infrared safe and compromises a future meaningful comparison with pQCD calculations at NNLO. Figure 1 shows

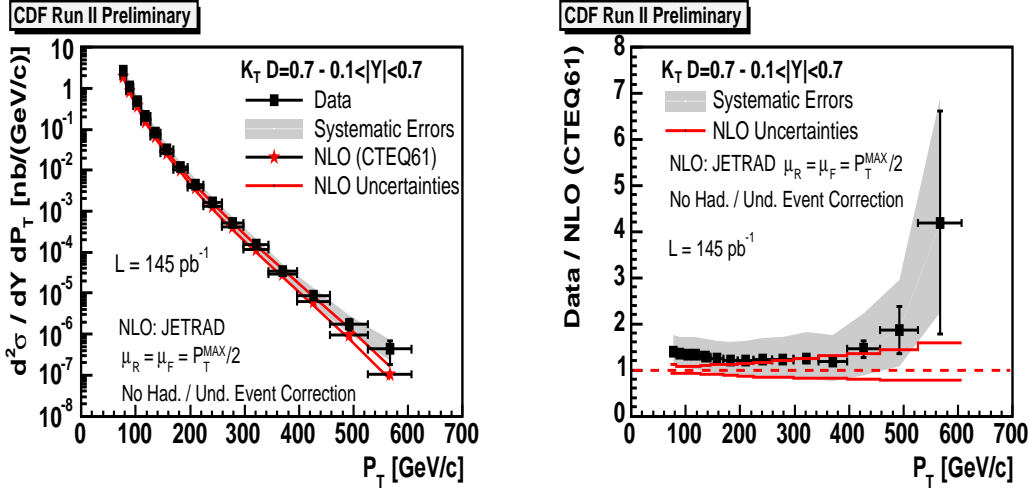


Figure 1: *The measured inclusive jet cross section compared to pQCD NLO predictions. Jets are searched for using the longitudinally invariant  $K_T$  algorithm.*

the measured inclusive jet cross section by CDF using the longitudinally invariant  $K_T$  algorithm [1] and based on the first  $145 \text{ pb}^{-1}$  of Run II data. Measurements have been performed using values for the D parameter in the  $K_T$  expression,

$$K_{ij} = \min(p_{T,i}^2, p_{T,j}^2) \cdot \frac{(y_i - y_j)^2 + (\phi_i - \phi_j)^2}{D}, \quad (1)$$

equal to 0.5, 0.7 and 1.0. The measurements are compared to pQCD NLO calculations [2] using CTEQ6 [3] parton density functions in the proton and antiproton and the renormalization and factorization scales set to  $p_T^{\text{max}}/2$ . The measured cross section is reasonably well described by the predictions for  $P_T^{\text{jet}} > 150 \text{ GeV}$  within the present uncertainties. The systematic errors on the data are dominated by the uncertainty on the jet energy scale determination while the theoretical predictions suffer from our limited knowledge of the gluon distribution at high  $x$ . At lower  $P_T^{\text{jet}}$ , the data is systematically above the predictions and the effect increases as D increases (see Figure 2). This indicates the presence of soft-gluon contributions and fragmentation effects that have not been taken into account yet.

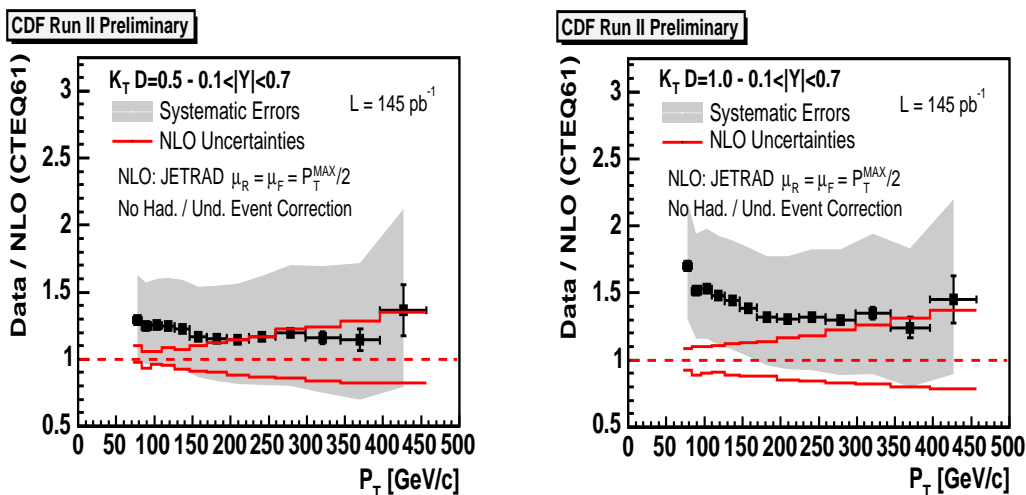


Figure 2: *Ratio between the measured inclusive jet cross section and the pQCD NLO predictions using the  $K_T$  algorithm with  $D=0.5$  and  $D=0.7$ , respectively.*

Figure 3 shows the measured inclusive jet cross section by D0 based on the first  $143 \text{ pb}^{-1}$  of Run II data. The new midpoint[4] jet algorithm has been used with a cone size  $R=0.7$ . This algorithm constitutes an improved version of the cone-based algorithm used in Run I and it is shown to be infrared safe in fixed-order parton-level calculations. The data is in good agreement with the pQCD NLO predictions using CTEQ6 parton density functions and  $R_{\text{sep}} = 1.3$  [5]. However, the measurement is dominated by a relatively large uncertainty on the absolute jet energy scale.

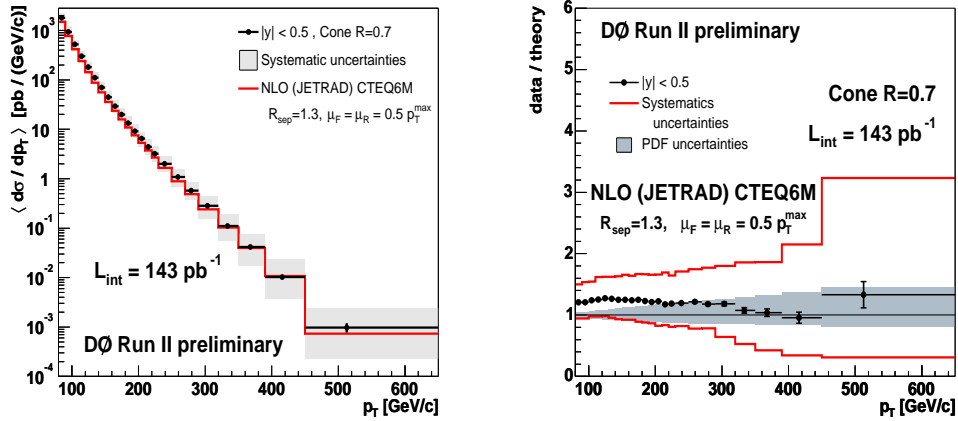


Figure 3: *The measured inclusive jet cross section by D0 compared to pQCD NLO predictions. Jets are searched for using the midpoint jet algorithm.*

Figure 4 shows the measured cross section by D0 as a function of the dijet invariant mass in dijet production of central jets. This measurement is particularly sensitive to the presence of narrow resonances decaying into jets of hadrons up to masses of 1.3 TeV. The data is well described by pQCD NLO predictions.

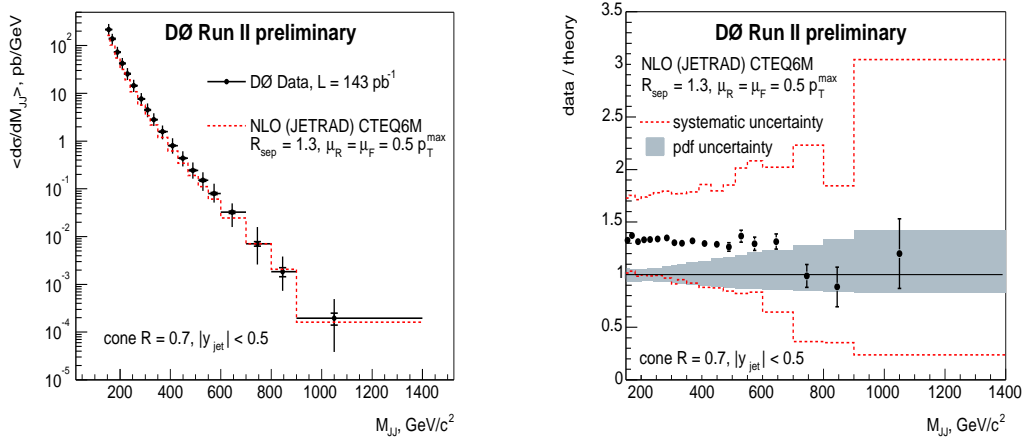


Figure 4: *The measured inclusive dijet cross section by D0 as a function of the dijet mass compared to pQCD NLO predictions.*

Nowadays, the Tevatron high- $P_T^{\text{jett}}$  jet data is used, together with prompt-photon data from fixed target experiments, to constrain the gluon distribution at high  $x$ . Jet measurements at large rapidities are important because they constrain the gluon density in a region in  $P_T^{\text{jett}}$  where no effect from new physics is expected.

The D0 experiment has already extended the jet cross section measurements to the forward region for jets with  $|Y^{\text{jet}}| < 2.4$  (see Figure 5). At the moment, the results are affected by large systematic errors. In the near future the experiments will highly reduce their uncertainties and precise cross section measurements will allow to further constrain the gluon distribution, and enhance their sensitivity to new physics at very high  $P_T^{\text{jet}}$ .

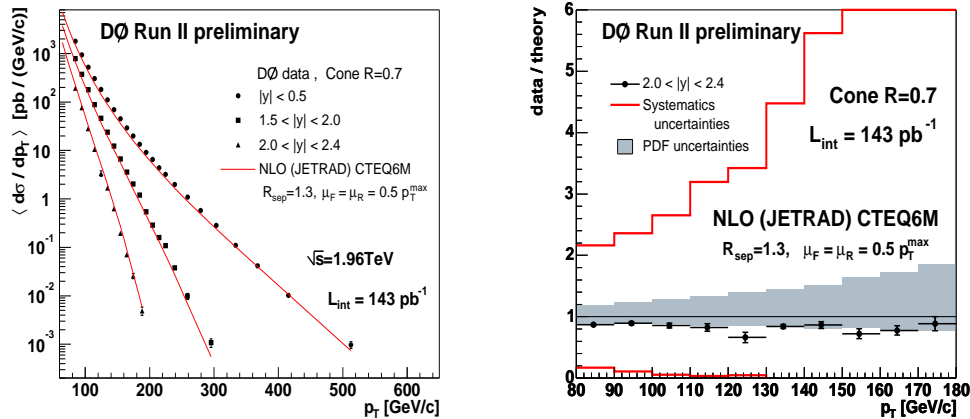


Figure 5: (Left) measured inclusive jet cross section by D0 in different regions of rapidity compared to pQCD NLO predictions. (Right) ratio between the measurements and the pQCD NLO predictions for jets with  $2.0 < |Y^{\text{jet}}| < 2.4$ .

### 3 Study of the Underlying Event

As mentioned in the previous section, the hadronic final states at 2 TeV are characterized by the presence of soft underlying emissions, usually denoted as *underlying event*, in addition to highly energetic jets coming from the hard interaction. The underlying event contains contributions from initial- and final-state soft gluon radiation, secondary semi-hard partonic interactions and interactions between the proton and anti-proton remnants that cannot be described by perturbation theory. These processes must be approximately modeled using Monte Carlo (MC) programs tuned to describe the data. The jet energies measured in the detector contain an underlying event contribution that has to be taken into account in order to compare the measurements to pQCD predictions. Hence, a proper understanding of this underlying contribution is crucial to reach the desired precision in the measured cross sections. In the analysis presented here, the underlying event in dijet production has been studied by looking at regions well separated from the leading jets, where the

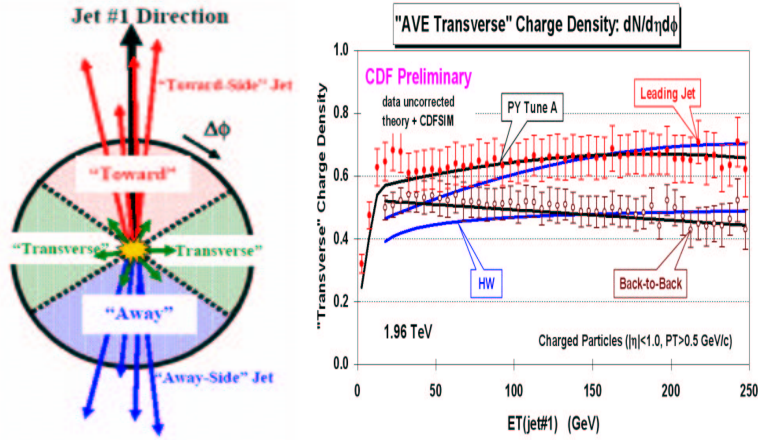


Figure 6: (Left) Scheme of the different  $\phi$  regions defined around the leading jet. (Right) Measured average track density in the transverse region as a function of the  $E_T^{\text{jet}}$  of the leading jet. The measurements are compared to different MC models.

underlying event contribution is expected to dominate the observed hadronic activity. Jets have been reconstructed using tracks with  $p_T^{\text{track}} > 0.5$  GeV and  $|\eta^{\text{track}}| < 1$  and a cone algorithm with  $R=0.7$ . The  $\phi$  space around the leading jet is divided in three regions: *toward*, *away* and *transverse* (see Figure 6-left), and the transverse region is assumed to reflect the underlying event contribution. Figure 6-right shows the average track density in the transverse region as a function of  $E_T^{\text{jet}}$  of the leading jet. Measurements are presented for the dijet inclusive sample and for events where the two leading jets are forced to be back-to-back in  $\phi$ , in order to further reduce extra hard-gluon radiation. The observed plateau indicates that the underlying event activity is, to a large extent, independent from the hard interaction. The measurements have been compared to the predictions from PYTHIA [6] and HERWIG [7] MC programs. The PYTHIA samples have been created using a special tuned set of parameters, denoted as PYTHIA-Tune A, which includes an enhanced contribution from initial-state soft gluon radiation and secondary parton interactions. It was determined as a result of similar studies of the underlying event performed using CDF Run I data [8]. PYTHIA-Tune A describes the hadronic activity in the transverse region while HERWIG underestimates the radiation at low  $E_T^{\text{jet}}$ . Similar measurements in Z+jet(s) events at high integrated luminosity will allow to explore the universality of the underlying event contribution, in events with a very different color configuration in the final state.

## 4 Jet Shapes

The internal structure of jets is dominated by multi-gluon emissions from the primary final-state parton. It is sensitive to the relative quark- and gluon-jet fraction and receives contributions from soft-gluon initial-state radiation and beam remnant-remnant interactions. The study of jet shapes at the Tevatron provides a stringent test of QCD predictions and tests the validity of the models for parton cascades and soft-gluon emissions in hadron-hadron collisions. The CDF experiment has presented results on jet shapes for central jets with transverse momentum in the region  $37 \text{ GeV} < P_T^{\text{jet}} < 380 \text{ GeV}$ , where jets are searched for using the midpoint<sup>1</sup> algorithm and a cone size  $R = 0.7$ . The integrated jet shape,  $\Psi(r)$ , is defined as the average fraction of the jet transverse momentum that lies inside a cone of radius  $r$  concentric to the jet cone:

$$\Psi(r) = \frac{1}{N_{\text{jet}}} \sum_{\text{jets}} \frac{P_T(0, r)}{P_T(0, R)}, \quad 0 \leq r \leq R \quad (2)$$

where  $N_{\text{jet}}$  denotes the number of jets. The measured jet shapes have been compared to the predictions from PYTHIA-Tune A and HERWIG MC programs. In

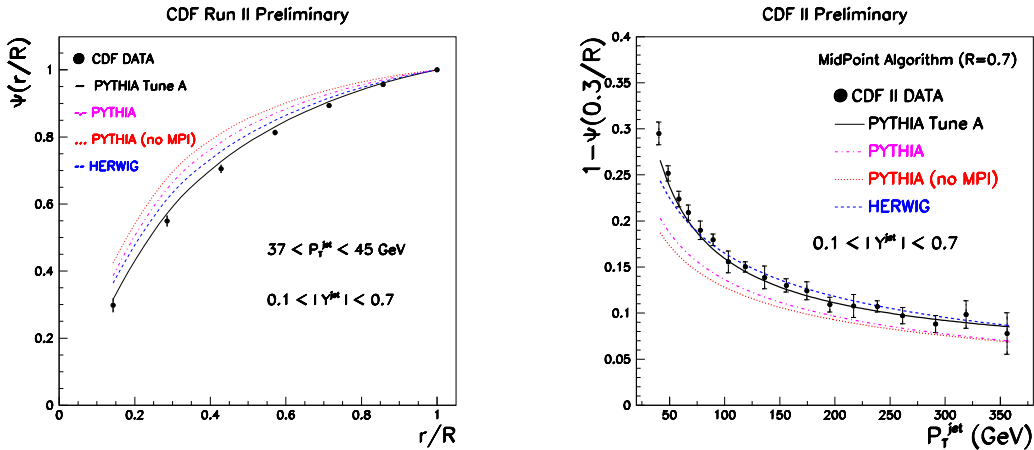


Figure 7: *The measured integrated jet shape compared to different MC predictions.*

addition, two different PYTHIA samples have been used with default parameters and with and without the contribution from multiple parton interactions (MPI) between proton and antiproton remnants, the latter denoted as PYTHIA-(no MPI), to

<sup>1</sup>A 75% merging fraction has been used instead of the default 50%.

illustrate the importance of a proper modeling of soft-gluon radiation in describing the measured jet shapes. Figure 7(left) presents the measured integrated jet shapes,  $\Psi(r/R)$ , for jets with  $37 < P_T^{\text{jet}} < 45$  GeV, compared to HERWIG, PYTHIA-Tune A, PYTHIA and PYTHIA-(no MPI) predictions. Figure 7(right) shows, for a fixed radius  $r_0 = 0.3$ , the average fraction of the jet transverse momentum outside  $r = r_0$ ,  $1 - \Psi(r_0/R)$ , as a function of  $P_T^{\text{jet}}$ . The measurements show that the fraction of jet transverse momentum at a given fixed  $r_0/R$  increases ( $1 - \Psi(r_0/R)$  decreases) with  $P_T^{\text{jet}}$ , indicating that the jets become narrower as  $P_T^{\text{jet}}$  increases. PYTHIA with default parameters produces jets systematically narrower than the data in the whole region in  $P_T^{\text{jet}}$ . The contribution from secondary parton interactions between remnants to the predicted jet shapes (shown by the difference between PYTHIA and PYTHIA-(no MPI) predictions) is relatively small and decreases as  $P_T^{\text{jet}}$  increases. PYTHIA-Tune A predictions describe all of the data well. HERWIG predictions describe the measured jet shapes well for  $P_T^{\text{jet}} > 55$  GeV but produces jets that are too narrow at lower  $P_T^{\text{jet}}$ .

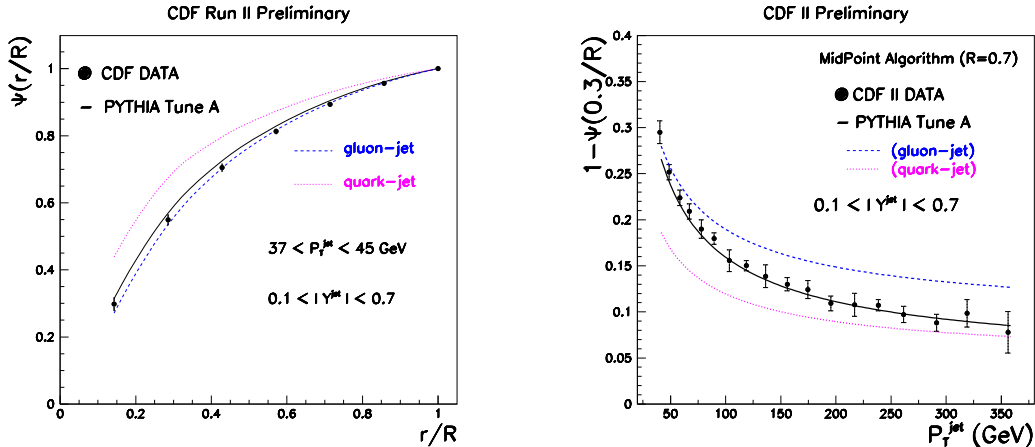


Figure 8: *The measured integrated jet shape compared to the predictions of PYTHIA-Tune A and the separated contributions from quark- and gluon-jets.*

Figure 8(left) shows the measured integrated jet shapes,  $\Psi(r/R)$ , for jets with  $37 < P_T^{\text{jet}} < 45$  GeV, compared to PYTHIA-Tune A and the predictions for quark- and gluon-jets<sup>2</sup> separately. Figure 8(right) shows the measured  $1 - \Psi(r_0/R)$ ,  $r_0 = 0.3$ , as a function of  $P_T^{\text{jet}}$ . The MC predictions indicate that the measured jet

<sup>2</sup>Each hadron-level jet from PYTHIA is classified as a quark- or gluon-jet by matching its directions with that of one of the outgoing partons from the hard interaction.



shapes are dominated by contributions from gluon-initiated jets at low  $P_T^{\text{jet}}$  while contributions from quark-initiated jets become important at high  $P_T^{\text{jet}}$ . This can be explained in terms of the different partonic contents in the proton and antiproton in the low- and high- $P_T^{\text{jet}}$  regions, since the mixture of gluon- and quark-jet in the final state partially reflects the nature of the incoming partons that participate in the hard interaction. For a given type of parton-jet in the MC (quark- or gluon-jet), the observed trend with  $P_T^{\text{jet}}$  shows the running of the strong coupling,  $\alpha_s(P_T^{\text{jet}})$ .

Jet shape measurements thus introduce strong constraints on phenomenological models describing soft-gluon radiation and the underlying event in hadron-hadron interactions. Similar studies with b-tagged jets will be necessary to test our knowledge of the b-quark jet fragmentation processes in hadron interactions, which is essential for future precise Top and Higgs measurements at the Tevatron and the LHC.

## 5 $\Delta\phi_{\text{dijet}}$ Decorrelations

The D0 experiment has employed the dijet sample to study azimuthal decorrelations,  $\Delta\phi_{\text{dijet}}$ , between the two leading jets. The normalized cross section:

$$\frac{1}{\sigma_{\text{dijet}}} \frac{d\sigma}{d\Delta\phi_{\text{dijet}}} \quad (3)$$

is sensitive to the spectrum of the gluon radiation in the event. The measurements have been performed in different regions of the leading jet  $P_T^{\text{jet}}$  starting at  $P_T^{\text{jet}} > 75$  GeV, and where the second jet is required to have at least  $P_T^{\text{jet}} > 40$  GeV. Figure 9 shows the measured cross section compared to LO and NLO predictions from NLOJET++ program [9]. The LO predictions, with at most three partons in the final state, is limited to  $\Delta\phi_{\text{dijet}} > 2\pi/3$ , for which the three partons define a *Mercedes-star* topology. It presents a prominent peak at  $\Delta\phi_{\text{dijet}} = \pi$  corresponding to the soft limit for which the third parton is collinear to the direction of the two leading partons. The NLO predictions, with four partons in the final state, describes the measured  $\Delta\phi_{\text{dijet}}$  distribution except at very high and very low values of  $\Delta\phi_{\text{dijet}}$  where additional soft contributions, corresponding to a resummed calculation, are necessary. A reasonable approximation to such calculations is provided by parton shower MC programs. Figure 10 presents the measured cross section compared to PYTHIA-Tune A, PYTHIA and HERWIG predictions in different regions of  $P_T^{\text{jet}}$ . PYTHIA with default parameters underestimates the gluon radiation at large angles. PYTHIA-Tune A predictions, which include an enhanced contribution from initial-state soft gluon radiation and secondary parton interactions, describe the azimuthal

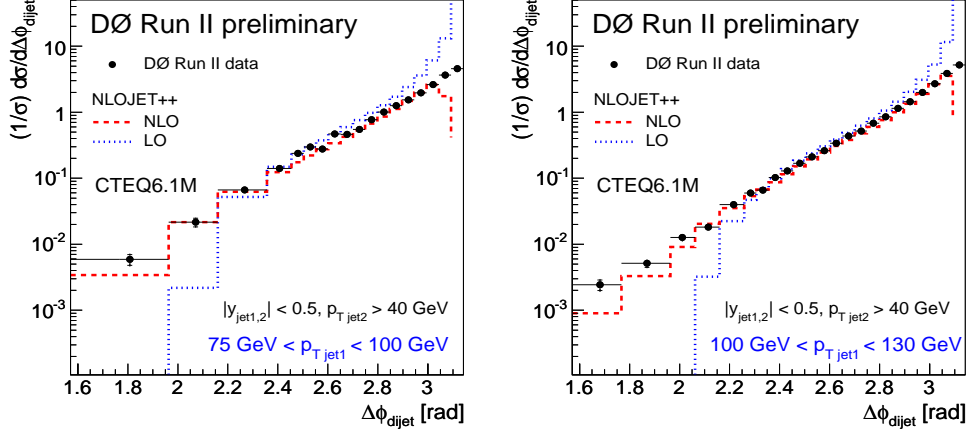


Figure 9: Measured azimuthal decorrelations in dijet production for central jets compared to  $p$ QCD predictions in different regions of the leading jet  $P_T^{\text{j}et}$ .

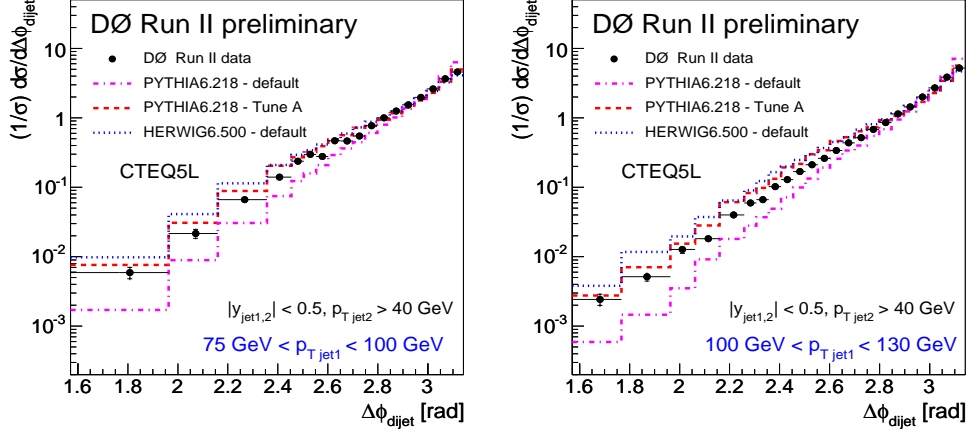


Figure 10: Measured azimuthal decorrelations in dijet production compared to  $PYTHIA$  and  $HERWIG$  predictions as a function of the leading jet  $P_T^{\text{j}et}$ .

distribution. HERWIG also describes the data although it tends to produce less radiation than PYTHIA-Tune A close to the direction of the leading jets.

## 6 W+jet(s) Production

A detailed study of hard processes involving the associated production of a W boson and a given number of jets in the final state is a main goal of the CDF physics program in Run II. These processes constitute the biggest background to Top and Higgs production in hadron colliders. Therefore, precise measurements of  $W+N_{\text{jets}}$  cross sections will be essential to test the LO and NLO QCD calculations used in order to estimate QCD-related backgrounds to Top and Higgs signals. During

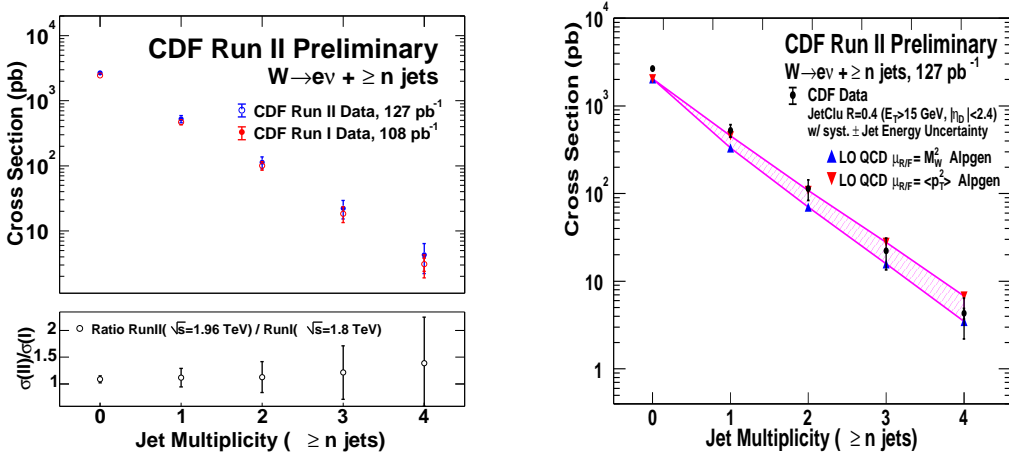


Figure 11: *Measured inclusive cross section for  $W + \geq N_{\text{jet}}$  production compared to Run I results and pQCD LO predictions as implemented in ALPGEN+HERWIG.*

the last years a number of new Boson+ $N_{\text{jet}}$  LO programs have become available [10] which include larger jet multiplicities in the final state, in addition to NLO calculations for the W+dijet case. These different programs are being interfaced to parton-shower models using different matching procedures to avoid double counting in the gluon radiation. Figure 11 shows the measured inclusive cross section for  $W + \geq N_{\text{jet}}$  production by CDF based on  $127\text{pb}^{-1}$  of Run II data. Jets with  $E_T^{\text{jet}} > 15 \text{ GeV}$  and  $|\eta^{\text{jet}}| < 2.4$  have been considered, where jets are searched for using the Run I cone algorithm with  $R = 0.4$ . The measurements are compared to similar results from Run I [11] and pQCD LO predictions for  $W + N_{\text{partons}}$  as implemented in ALPGEN interfaced to the parton cascades and fragmentation from HERWIG. The measured cross section in Run II is about  $\sim 10\%$  larger than that in Run I thanks

to the new centre-of-mass energy. The relative rates as a function of jet multiplicity are similar to those observed in Run I which indicates that the  $W$  cross section is reduced by  $\sim 80\%$  per each jet required. The pQCD LO predictions describe the data well but suffer from large uncertainties due to the strong dependence on the hard scale used in the calculation.

Figure 12 present the measured  $E_T^{\text{jet}}$  spectrum for the  $N^{\text{th}}$  jet in  $W + \geq N_{\text{jet}}$

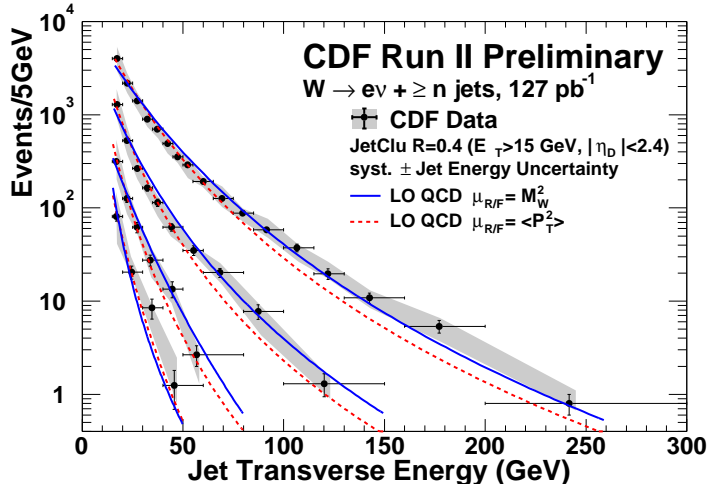


Figure 12: Measured  $E_T^{\text{jet}}$  spectrum for the  $n^{\text{th}}$  jet in  $W + \geq N_{\text{jet}}$  production compared to pQCD LO predictions as implemented in ALPGEN interfaced to HERWIG.

production. The spectrum for the least energetic jet is sensitive to the details of the interface between the pQCD LO calculation and the parton shower evolution. The measured spectrum is in agreement with the predictions from ALPGEN+HERWIG within the present uncertainties. In the data the systematic errors are dominated by the jet energy scale determination while the LO theoretical predictions present a strong dependence on the selected renormalization and factorization scales.

As the recorded luminosity of the experiments increases, precise measurements for  $W + b\bar{b}$  production will be possible. Those measurements will be compared to pQCD NLO calculations with much reduced theoretical uncertainties.

## 7 $\gamma +$ Heavy Flavor Jet Production

The CDF experiment has presented measurements of cross sections for the production of high- $E_T$  photons in association with heavy quark jets, based on the first  $66 \text{ pb}^{-1}$  of Run II data. Those processes can signal the presence of new physics like,

for example, stop production when they are produced together with large missing transverse energy in the detector. In addition, these cross sections directly probe the heavy quark contents in the proton. Displaced secondary vertices, coming from the

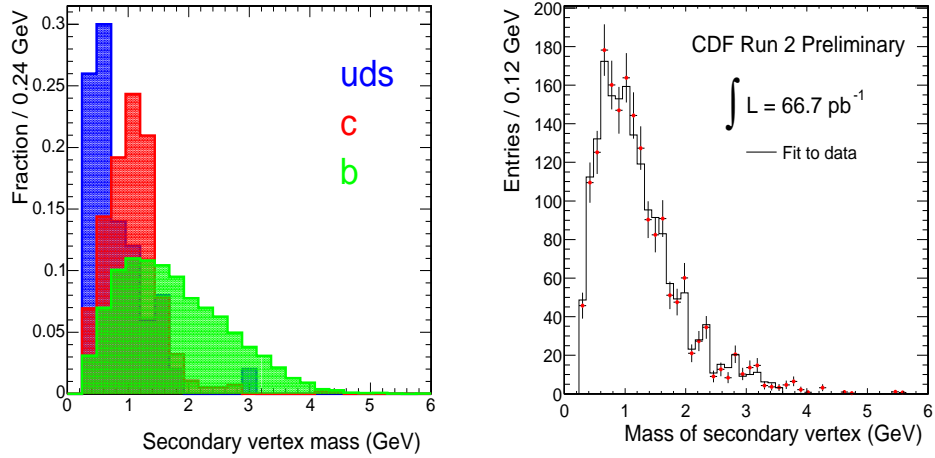


Figure 13: (Left) secondary mass distributions for  $b/c$  and  $uds$  quarks determined from MC. (Right) fit to the measured mass distribution in data using MC templates.

decay of long-lived charm and bottom hadrons and reconstructed in the CDF silicon tracker, are used in order to identify jets coming from heavy quarks. The mass

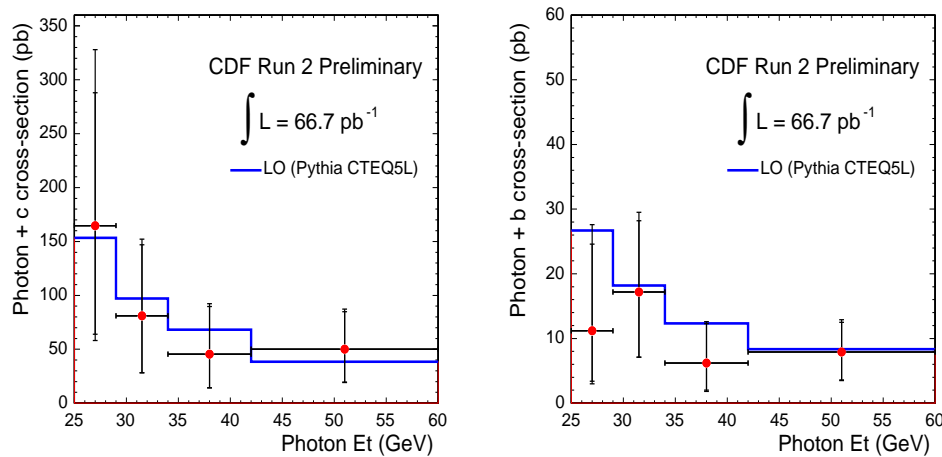


Figure 14: Measured  $\gamma + b$ -jet and  $\gamma + c$ -jet cross sections compared to LO pQCD.

of the observed secondary vertex is employed to separate the different contributions from charm, bottom and light quarks (the latter producing fake tags) to the sample of heavy-quark jet candidates. Monte Carlo templates are fitted to the measured

secondary vertex mass distribution in the data (see Figure 13) to extract the different contributions and use them to compute the cross sections. Figure 14 shows the measured cross sections for  $\gamma + c - \text{jet}$  and  $\gamma + b - \text{jet}$  production compared to LO QCD predictions as implemented in PYTHIA. The measurements are in agreement with the predicted cross section within the still limited statistics in the data.

## 8 Acknowledgments

I thank PIC'04 organizers for their invitation, help and kindness during the conference in Boston and for the exciting program of talks and discussions they made possible.

## References

1. Stephen D. Ellis, Davision E. Soper, Phys.Rev. D48 (1993) 3160-3166.
2. W.T. Giele, E.W.N. Glover, D. A. Kosower, Nucl. Phys. B403 (1993) 633-670.
3. J. Pumplin et al., JHEP 0207 (2002) 012.
4. G. C. Blazey, et al., hep-ex/0005012.  
S.D. Ellis, J. Huston and M. Toennesmann, hep-ph/0111434.
5. S. D. Ellis, Z. Kunszt, D. E. Soper, Phys.Rev.Lett. 69 (1992) 3615-3618.
6. H.-U. Bengtsson and T. Sjöstrand, Comp. Phys. Comm. 46 (1987) 43.
7. G. Marchesini et al., Comp. Phys. Comm. 67 (1992) 465.
8. D. Acosta et al., CDF Collaboration, Phys. Rev. D65, 092002, (2002).
9. Zoltán Nagy, Zoltán Trócsányi, Phys.Rev.Lett. 79 (1997) 3604-3607.
10. M. Mangano et al.: 'ALPGEN', preprint hep-ph/0206293.  
E. Boss et al.: 'CompHEP', preprint hep-ph/9503280.  
S. Tsuno et al.: 'GR@PPA', preprint hep-ph/0204222.  
F. Maltoni and T. Stelzer: 'MADGRAPH', preprint hep-ph/0208156.  
K. Ellis and J. Campbell: 'MCFM', preprint hep-ph/0202176.
11. T. Affolder et al., The CDF Collaboration, Phys. Rev. D63 (2001) 072003.